Deglacial–Holocene Svalbard paleoceanography and evidence of Melt Water Pulse 1B

Skye Yunshu Tian,[1*] Moriaki Yasuhara,[1*] Yuanyuan Hong,[1*] Huai-Hsuan M. Huang,[1,2] Hokuto Iwatani, [1,3] Wing-Tung Ruby Chiu,[1] Briony Mamo,[1] Hisayo Okahashi,[1] Tine L. Rasmussen[4]

[1]School of Biological Sciences and Swire Institute of Marine Science, the University of Hong Kong, Kadoorie Biological Sciences Building, Pokfulam Road, Hong Kong SAR, China.

[2]GeoZentrum Nordbayern, Universität Erlangen-Nürnberg, Loewenichstraße 28, D-91054 Erlangen, Germany.

[3]Division of Earth Science, The Graduate School of Sciences and Technology for Innovation, Yamaguchi University, Yoshida 1677-1, Yamaguchi 753-8511 Japan.

[4]CAGE – Centre for Arctic Gas Hydrate, Environment and Climate, Department of Geology, UiT The Arctic University of Norway, Dramsveien 201, 9037 Tromsø, Norway.

[*]To whom correspondence should be addressed.

Emails: moriakiyasuhara@gmail.com; u3514102@connect.hku.hk; oocirclr@gmail.com

Key words: The last deglaciation; Holocene; Sea level change; neoglaciation;

Paleoceanography; Arctic Ocean; Micropaleontology; Ostracoda.

Abstract

Better understanding of deglacial meltwater pulses (MWPs) is imperative for future predictions of human-induced warming and abrupt sea-level change because of their potential for catastrophic damage. However, our knowledge of the second largest meltwater pulse MWP-1B that occurred shortly after the start of the Holocene interglacial remains very limited. Here, we studied fossil ostracods as paleoenvironmental indicators of water depth, salinity, and temperature in two marine sediment cores from Storfjorden, Svalbard margin (the Arctic Ocean), to investigate near-field (i.e. areas located beneath continental ice sheets at the Last Glacial Maximum) evidence of MWP-1B. The depositional environment changed from a cold bathyal environment to a warmer bathyal environment at ~11,300 yr BP indicating incursion of warm Atlantic water into the Nordic seas, and eventually to a cold neritic environment by ~11,000 yr BP because of melting of the Svalbard-Barents Sea ice sheet and resultant isostatic rebound. This process corresponds to rapid relative sea-level fall of 40-80 m of MWP-1B from ~11,300 to 11,000 yr BP.

1. Introduction

The last deglaciation-Holocene is one of the most studied periods in Earth history due to its importance for understanding short-term evolution of global climate in relation to oceanographic and glacial conditions in high-latitude regions of the northern hemisphere. During the main phase of deglaciation from 16,500 to 8200 yr BP, regional to global warming triggered the rapid decay of large ice sheets and massive discharge of meltwater, which contributed to total eustatic sea-level rise of ~120 meters (Lambeck

et al., 2014). The middle to late Holocene is characterized by gradual cooling and climatic deterioration (Mayewski et al., 2004), and global sea levels showed minor rises occurring at progressively slower rates until they approached modern values (Lambeck et al., 2014). During the late Holocene, Neoglacial cooling culminated in ice sheet advance under the background of declining insolation (Mayewski et al., 2004).

During the overall main deglaciation phase, two events of abrupt sea level rise known as meltwater pulses (MWPs) 1A and 1B occurred, superimposed on the secular, gradual background rise. Post-glacial global sea-level rise has been reconstructed primarily based on tropical coral-reef cores, because low-latitude regions (far-field) have experienced mostly eustatic effects with minimal isostatic effects on the sea level change (Milne and Mitrovica, 2008; Stanford et al., 2011; Yokoyama et al., 2018). While MWP-1A at 14,500–14,000 yr BP is distinct and well-documented, MWP-1B is elusive in far-field sea-level records (Lambeck et al., 2014; Harrison et al., 2019). Since Fairbanks (1989) first identified MWP-1B at 11,300 yr BP from Barbadian coral reef cores, the timing, magnitude and even existence of MWP-1B have been debated and currently remain inconclusive. This is despite the acquisition and analysis of new, high-quality coral reef cores from key regions including Tahiti and the Great Barrier Reef, possibly because depth uncertainties of coral habitat (approximately 6 m) make it difficult to reconstruct and interpret far-field MWP-1B that is in relatively small magnitude (14±2 m) in short duration against continuous deglacial sea level rise. (Bard et al., 1996; Bard et al., 2010; Stanford et al., 2011; Abdul et al., 2016; Yokoyama et al., 2018). Another major criticism is that, to date, evidence for MWP-1B within marine sediments from the Southern Ocean or North Atlantic adjacent to the relevant ice sheets, the source of the meltwater, has been lacking (Bard et al., 2010).

A high-latitude (near-field) ocean should have experienced MWP-1B-induced environmental changes if MWP-1B existed. Likely changes are especially water-depth decrease (relative sea-level fall) due to isostatic rebound from ice-sheet loss overwhelming eustatic sea-level rise (see the next section) as well as cooling and salinity change induced by meltwater runoff. Ostracods (small crustaceans with calcite shells) are known to be sensitive to environmental changes including changes in water depth, temperature, and salinity (Cronin, 1981; Yasuhara and Seto, 2006; Cronin, 2015; Gemery et al., 2017; Hong et al., 2019; Stepanova et al., 2019). Here we investigate fossil ostracods in two sediment cores (JM10-10GC, 77.41˚N, 20.10˚E, water depth 123 m; JM10-12GC, 77.12˚N, 19.41˚E, water depth 146 m) from Storfjorden Sound (Fig. 1), Svalbard, and provide evidence of MWP-1B during the final stages of deglaciation. Penetration of the warm Atlantic water into the Nordic seas melted the covering ice sheets ~11,300 years ago and the isostatic rebound associated with MWP-1B resulted in an abrupt relative sea level fall between ~11,300-11,000 yr BP on the Svalbard margin. Neoglacial cooling and glacier advance likely commenced at ~2000 yr BP with oceanographic and glacial conditions becoming more unstable.

2. Oceanographic and geologic setting

Storfjorden is a sound which extends from 76 to 80˚N in the southeastern part of the Svalbard archipelago (Fig. 1). It is open to the south and is bordered by Spitsbergen to the west and Barentsøya and Edgeøya to the northeast, where two passages connect the sound to the Arctic Ocean. Warm Atlantic water of the West Spitsbergen Current runs northward along the western slope of Svalbard and a small branch enters Storfjorden (Skogseth et al., 2004; Rasmussen and Thomsen, 2015). Cold polar water of the East

Spitsbergen Current also enters Storfjorden (Skogseth et al., 2004; Rasmussen and Thomsen, 2014). There is an inner deep basin (maximum water depth ~190 m) connected to shallow shelves (~40 m) to the north and the east, and a 120 m deep sill in the south that separates it from the Storfjorden Trough (Rasmussen and Thomsen, 2015). From December to July, seasonal sea ice covers the sound and wind from the northeast blows ice to create large polynyas on the shelf east of the deep basin (Skogseth et al., 2005; Rasmussen and Thomsen, 2015). Recurrent freezing and salt rejection in the polynyas produce cold (-1.9 ℃) and salty (>34.8) brine, which sinks into the inner basin and eventually overflows the sill into the Storfjorden Trough (Skogseth et al., 2004; Rasmussen and Thomsen, 2015; Knies et al., 2016).

In near-field regions, the timing and magnitude of post-glacial glacio-isostatic uplift and resultant relative sea-level fall is controlled by the distribution of past ice loading and deglacial history (Khan et al., 2015). Areas beneath and surrounding a substantial ice load were subject to the greatest glacioisostatic depression and then greatest uplift when major retreat or rapid disintegration of ice sheets occurred (Khan et al., 2015; Harrison et al., 2019). The Svalbard-Barents Sea Ice Sheet formed part of the Eurasian ice sheet complex (Patton et al., 2017) during the Last Glacial Maximum (LGM), and extensively covered Svalbard in the northwest. It exhibited spatio-temporally dynamic patterns of ice retreat during the last deglaciation to early Holocene followed by ice readvances since the late Holocene (Ingolfsson and Landvik, 2013; Farnsworth et al., 2018). Recent studies recognize it as an instable, multi-domed ice sheet with one of the large ice domes located on easternmost Spitsbergen or northeastern Svalbard near our study sites (Dowdeswell et al., 2010; Hogan et al., 2010; Ingolfsson and Landvik, 2013). Ice sheet thinning commenced in the southern and western Svalbard before circa 20,000

yr BP and progressed to northern and eastern Svalbard, with different phases of major retreat correlative with abrupt warming events (e.g. Bølling-Allerød warming) and warm Atlantic water incursions (Gjermundsen et al., 2013; Ingolfsson and Landvik, 2013; Łącka et al., 2015; Nielsen and Rasmussen, 2018). The ice front may not retreated from northern Svalbard until the earliest Holocene and some recent studies show spatial variation in timing of final retreat ranging from 11,600 to 11,300 yr BP (Gjermundsen et al., 2013; Flink et al., 2017; Nielsen and Rasmussen, 2018).

3. Materials and Methods

3.1. Sample processing

We studied two cores JM10-10GC and JM10-12GC from the Storfjorden inner basin. Age models of these cores are based on AMS ^{14}C dates and from Rasmussen and Thomsen (2014). All AMS ^{14}C dates were calibrated to calendar ages using the Calib7.02 and the Marine13 programs (Rasmussen and Thomsen, 2014). Sedimentation rate is relatively uniform in both cores except for a hiatus between 345.5 cm and 324.5 cm (9500–6500 yr BP) in Core JM10-10GC (Rasmussen and Thomsen, 2014). Core JM10-10GC (403 cm long) was taken from 123 m water depth in a sub-basin east of the main basin (Rasmussen and Thomsen, 2014) (Fig. 1). The 320-cm-long Core JM10-12GC was taken on the northern flank of the sill at a water depth of 146 m (Rasmussen and Thomsen, 2014) (Fig. 1). Cores JM10-10GC and JM10-12GC were sub-sampled at 5 cm and 4 cm intervals respectively. All sedimentary sub-samples were wet sieved with mesh sizes of 63, 100 and 1000 μm, oven dried, and then dry sieved over mesh-size of 150 μm, the standard fraction for fossil ostracod research (Gemery et al., 2017; Yasuhara et al., 2017). Specimens smaller than 150 μm are usually early molt stage

juveniles that are difficult to identify. We used a standard counting method that counts every articulated carapace as two specimens and isolated valves as one (Yasuhara et al., 2017).

3.2. Multivariate analysis, Mutual Ostracod Depth Range (MODR), and Mutual Ostracod Salinity Range (MOSR)

Multivariate statistical analyses including Q-mode K-means clustering and Species Indicator Value were used to show temporal variation of ostracod faunal composition. We combined species relative abundance data (%) of two cores in multivariate analyses considering inter-core similarity and consistency. We performed sample cutoff and species cutoff on fossil assemblages to exclude samples with less than 10 specimens and rare species that has a negative lower boundary of 95% cluster confidence interval (Bennington and Rutherford, 1999). After these cutoffs, there are 5492 specimens that belong to 30 species from 128 samples included in multivariate analyses, taking up 96% of total number of specimens. The mechanism of Q-mode k-means clustering is to divide samples into clusters so that species composition difference is maximized across clusters and minimized within clusters (Hartigan and Wong, 1979; Dimitriadou et al., 2002). Simple Structure Index was used to determine the optimal number of clusters (i.e. four clusters in this case) (Hartigan and Wong, 1979). The post-hoc species indicator value method quantifies the fidelity and specificity of species in relation to each cluster, and it is used to calculate indicator values of each species for each cluster and identify significant indicator species of each cluster with permutation testing (Dufrêne and Legendre, 1997).

The Mutual Ostracod Depth Range (MODR) and Mutual Ostracod Salinity Range (MOSR) methods are analogous to the Mutual Ostracod Temperature Range (MOTR) method developed by Horne (2007) and were used to semi-quantitatively reconstruct paleo water depth and paleo salinity respectively in Svalbard, based on presence/absence of species in a fossil assemblage. Although water depth itself may impact ostracod assemblages through combined effects of a suite of environmental variables that co-vary with depth, ostracods in general exhibit relatively strict depth zonation and they can be used as a reliable proxy for qualitative to quantitative paleodepth reconstructions (Yasuhara et al., 2005; Yasuhara and Seto, 2006; Cronin, 2015; Cronin et al., 2017). The MODR and MOSR methods run in parallel here. Their mechanism is to find the mutual depth range/salinity range where depth/salinity range values of all species in a given sample overlap. The resulting mutual depth/salinity range is regarded as an estimation of paleo depth/paleo salinity for that sample. Sample and species cutoffs on fossil assemblages were conducted in the same way as described in the last paragraph. The Arctic Ostracode Database 2015 (AOD 2015) provided comprehensive modern data from which species' depth ranges and salinity ranges could be inferred (Gemery et al., 2017). Samples with <10 specimens or >500 m water depth were excluded from the database. For each species in the AOD 2015 dataset, its shallowest and deepest occurrences (number of specimens in a sample out of total number of specimens in all samples >1%) were identified and the range between them is considered as the species depth range. The species salinity range is determined in the same way as that of the depth range. Noticeably, *Cytheropteron montrosiense* and *Loxoconcha* sp. which coexisted within Cluster D before 11,300 yr BP are possibly transported from shallow-marine areas with ice rafted debris. The occurrence of such shallow-living species in glaciomarine sediments has been reported before by Cronin

(1981); Schoning and Wastegård (1999). Therefore, these two species are not considered in the water depth reconstruction. Two examples of paleo water depth estimation with the MODR method are shown in Figure 2.

4. Results

We studied 82 samples from Core JM10-10GC and 75 samples from JM10-12GC and found 5719 specimens and 52 species in total. Q-mode k-means clustering divided the JM10-10GC and JM10-12GC samples into four Clusters – A, B, C and D (Figs. 3 and 4). Indicator Value results revealed statistically significant indicator species for these clusters (Figs. 4–6; Table 1): Cluster A, *Acanthocythereis dunelmensis*, *Cytheropteron discoveria* and *Heterocyprideis fascis*; Cluster B, *Bythocythere constricta*, *Cluthia cluthae*, *Cytheropteron arcuatum*, *Cytheropteron paralatissimum*, *Cytheropteron tumefactum* and *Semicytherura concentrica*; Cluster C, *Elofsonella concinna*, *Normanicythere leioderma*, *Sarsicytheridea bradii* and *Sarsicytheridea punctillata*; and Cluster D, *Cytheropteron dimlingtonensis*, *Cytheropteron irizukii*, *Cytheropteron montrosiense* and *Cytheropteron pseudomontrosiense*. Cluster A characterizes the uppermost section of Core JM10-10GC spanning the past 2000 years (Fig. 3A). Although there is no sample in Core JM10-12GC representing Cluster A, the indicator species of Cluster A show a consistent increase in relative abundance in the uppermost sediments (Fig. 3B). Cluster B characterizes the lower and upper core sections that correspond to sediments older than ~11,000 and younger than 2000 yr BP respectively. Cluster C spans the middle of the cores between 11,000–2000 yr BP (Fig. 3), although Cluster B also intermittently occurs in this section. Cluster D exclusively occurs in the base of the two cores representing sediments older than 11,300 yr BP (Fig. 3).

Immediately after the disappearance of Cluster D and before the emergence of Cluster C, there is a short-term spike in *Krithe glacialis* occurrence from ~11,300 yr BP (Fig. 3). Quantitative reconstructed paleo water depths and paleo salinities of Cores JM10-10GC and JM10-12GC using the Mutual Ostracod Depth Range (MODR) and Mutual Ostracod Salinity Range (MOSR) methods are shown in Figures 7 and 8, respectively. The application of MOSR method to a given fossil assemblage is not always successful as salinity range values of some component species do not overlap and no mutual salinity range can be inferred for this fossil assemblage. In such case, one missing data horizon is introduced into the MOSR reconstruction as shown in Figure 8.

5. Discussion

Discovered from far-field marine sediment records, MWP-1B is currently understood to have resulted in a rapid global sea level rise of 14–20 m at ~11,300 yr BP, induced by the Northern Hemisphere ice-sheets loss (Fairbanks, 1989; Bard et al., 2010; Abdul et al., 2016). In the near-field regions under direct influence of the Svalbard-Barents Sea Ice Sheet, we hypothesize that MWP-1B would be recorded by the following environmental changes at ~11,300 yr BP: warming by penetration of warm Atlantic water; resulting melt of the covering and surrounding ice in the region; abrupt sea level fall due to isostatic uplift; and cooling and freshening by meltwater discharge. These predictions are clearly depicted in the sedimentological record when the autoecology of key species (summarized in Table 2) is applied to the rapid faunal turnovers from Cluster D through Cluster B to C (Figs. 3, 5 and 6). Cluster D is the pre-MWP-1B assemblage dating 13,500-11,300 yr BP and its most important indicator species, *Cytheropteron pseudomontrosiense*, (Figs. 3, 5 and 6) inhabits upper bathyal, low

temperature (0 to 8–12 °C) environments (Whatley and Masson, 1979; Cronin, 1981; Stepanova, 2006; Stepanova et al., 2019). This assemblage also almost completely lacks neritic species that are abundant in other clusters (Figs. 3, 5 and 6; Table 2). Cluster D therefore indicates an upper bathyal, very cold marine setting. The pre-MWP-1B assemblage rapidly declined at ~11,300 yr BP, meanwhile *Krithe glacialis* briefly emerged for approximately 200–300 years (Fig. 3). *Krithe glacialis* indicates deep but comparatively warmer environments than those of *Cytheropteron pseudomontrosiense*, because *Krithe glacialis* [see Yasuhara et al. (2014) for the taxonomic definition of this species] is known from uppermost bathyal depths of the Greenland Sea where temperatures are comparatively warm, but absent from deeper, colder waters (Whatley et al., 1996; Whatley et al., 1998). Furthermore, modern distribution of *Cytheropteron pseudomontrosiense* is mostly limited to the Arctic Ocean excluding the Greenland Sea (Stepanova et al., 2003). Thus, the occurrence of *Krithe glacialis* here indicates an uppermost bathyal environment and an influx of warm Atlantic water. It is noticeable that peaks of *Krithe glacialis* in two cores correlated well in time with abrupt increase in planktonic foraminifera abundance that is indicative of oceanic conditions (Fig. 9) (Rasmussen and Thomsen, 2015). Consistent with other marine sediment records showing abrupt and significant warming in this region at similar timing (i.e. ~11,000 BP) (Hald et al., 2004; Ebbesen et al., 2007), coeval peaks of *Krithe* and planktonic foraminifera strengthen our interpretation of warm Atlantic water incursion that may have region-wide impacts on the Svalbard-Barents Sea ice sheet. Following the ephemeral peaks of *Krithe glacialis*, indicator species of Cluster B and then C rapidly emerged from ~11,300 yr BP onwards by replacing Cluster D indicator species (Fig. 3). The most important indicator species of Cluster B, *Cytheropteron arcuatum*, and the indicator species of Cluster C, *Normanicythere leioderma*, *Sarsicytheridea bradii*,

Sarsicytheridea punctillata, and *Elofsonella concinna*, are all cold, neritic species that are widely distributed in subarctic to Arctic regions (Stepanova, 2006; Stepanova et al., 2007; Stepanova et al., 2012; Gemery et al., 2017; Stepanova et al., 2019). Indeed, these species often coexist in both Cluster B and C samples (Figs. 3, 5 and 6). Their ecological preferences differ in that *Cytheropteron arcuatum* is a comparatively deeper species (lower neritic) than the indicator species of Cluster C (Fig. 3 and Table 2) (Stepanova et al., 2019). The Cluster D–*Krithe*–Cluster B–Cluster C succession reflects environmental changes related to MWP-1B as follows (Fig. 3; Table 3): (1) The region was an upper bathyal environment >11,300 yr BP before MWP-1B, (2) warm Atlantic water influx rapidly melted the Svalbard-Barents Sea ice sheet and triggered MWP-1B at ~11,300 yr BP, (3) MWP-1B meltwater cooled the sea water and sudden ice-sheet loss caused rapid relative sea-level fall (regional uplift/rebound), changing the depositional environment from an upper bathyal setting to neritic setting. The timing of the end of this succession slightly varies between the two cores (11,000–10,500 yr BP), but Core JM10-12GC has higher time resolution in this section and the Cluster B/C boundary in this core is at ~11,000 yr BP. Thus the MWP-1B-induced environmental changes recorded in this study started from 11,300 and ended at 11,000 yr BP abruptly, consistent with previous proposals of MWP-1B timing and our hypotheses of MWP-1B occurrence in near field regions (Fairbanks, 1989; Lambeck et al., 2014; Yokoyama et al., 2018). It is important to know the timing of MWP-1B relative to the Younger Dryas (YD) (ended at 11,700 yr BP) precisely. Although it is difficult to ascertain a few hundred years difference from a marine sediment core, several cores with independent age models [this study; Hald et al. (2004); Ebbesen et al. (2007)] consistently indicate warm Atlantic water incursion at ~11,000 yr BP and, thus, MWP-1B likely occurred after the termination of the YD.

Field-based reconstructions (e.g., based on raised beaches, glacial sediments and glacial landforms) and modelling of the deglacial history in Svalbard generally support our inference that the abrupt sea-level fall in Storfjorden was caused by isostatic adjustment during late stage ice retreat (Auriac et al., 2016; Nielsen and Rasmussen, 2018). Northern and eastern Svalbard fully deglaciated during the YD – earliest Holocene, and this was possibly in phase with the decay of the large ice dome in easternmost Spitsbergen thus triggering regional postglacial rebound (Dowdeswell et al., 2010; Flink et al., 2017; Nielsen and Rasmussen, 2018). Post-glacial uplift curves constructed from dated raised beaches provide direct evidence of the relative sea-level fall associated with the postglacial rebound (Forman et al., 2004; Ingolfsson and Landvik, 2013). However, they are of relatively low time-resolution, and cannot be compared with the MWP-1B timing precisely. Thus, our ostracod evidence of the abrupt relative sea-level fall from well-dated marine sediment cores provides a key piece of the puzzle of MWP-1B.

Quantitative water-depth reconstruction is in accordance with the above-discussed scenario by showing conspicuous, abrupt relative sea level fall at the time of MWP-1B (Table 3; Fig. 7). Because the present water depths of Sites JM10-10GC and JM10-12GC are 123 m and 146 m, respectively, which approximates the maximum depth of the upper part of each core estimated by the MODR method, we consider that the maximum depth (orange plots in Fig. 7, A and B) represents actual paleo-depth. General underestimation of water depths may be due to the continuous presence of euryhaline species that adapt to relatively wide ranges of water depths and salinities across the neritic zone (see discussion in the next section). The magnitude of the decrease in water-depth from pre- to post-MWP-1B is estimated to be ~40–80 m by the MODR method

(Fig. 7), which is consistent with our interpretation of ostracod faunal change from Cluster D to Cluster B/C (as discussed above; Table 3) and also coarser time-resolution reconstructions from raised beaches (Forman, 1990; Bondevik et al., 1995; Forman et al., 2004; Long et al., 2012).

During ~11,000–2000 yr BP, Cluster C indicator species (*Elofsonella concinna*, *Normanicythere leioderma*, *Sarsicytheridea bradii* and *Sarsicytheridea punctillata*) have dominated (Figs. 3, 5 and 6). They are all cold neritic species (Cronin, 1981; Gemery et al., 2017), but have different salinity preferences (Stepanova, 2006; Stepanova et al., 2007; Stepanova et al., 2012; Stepanova et al., 2019). *Normanicythere leioderma* is a fully marine species; *Sarsicytheridea bradii* (salinity 6.5 to >30), *Elofsonella concinna* (salinity >16), and *Sarsicytheridea punctillata* (salinity 3.8 to >30) are euryhaline species that tolerate low salinities in shallower neritic zone with fresh water discharge (Stepanova et al., 2019). From YD-Holocene transition to early Holocene, development of low-salinity conditions indicated by the Cluster C assemblage is not unexpected in Storfjorden since the depositional environment changed from a deep bathyal setting to a shallow neritic setting, possibly under the greater influence of fresh surface water. Furthermore, inflow of warm and saline Atlantic water may be weaker after the major incursion event between 11,300-11,000 yr BP and local hydrology may be more dominated by cold and fresh Arctic water (Cronin et al., 2012; Rasmussen et al., 2012; Rasmussen and Thomsen, 2014; Rasmussen and Thomsen, 2015). Freshening during ~11,000-2000 yr BP as inferred above is semi-quantitatively illustrated by MOSR reconstruction in Figure 8. Maximum and minimum estimations of paleo salinities both represent rapid decline across the MWP-1B interval from high values before 11,300 yr BP to relatively low values

between ~11,000-2000 yr BP, despite slight timing offset between two cores. Large (small) difference between the maximum and minimum salinity estimations before (after) 11,300 yr BP likely reflects short-term (e.g., seasonal or inter-annual) salinity variability. As ice had already retreated from the Storfjorden inner basin during the YD-Holocene transition (Nielsen and Rasmussen, 2018), the nearby large ice dome may have been relatively stable during ~11,000-2000 yr BP with insignificant meltwater discharge into Storfjorden as evident from generally low IRD content. In summary, paleoceanographic conditions were probably cold and slightly fresher with an inactive ice-sheet condition in this long, stable interval.

The uppermost core sediments (after ~2000 yr BP) are characterized by the prevalence of Cluster A and B indicator species and the disappearance of Cluster C indicator species (Figs. 3, 5 and 6; Table 2). This succession indicates the establishment of modern conditions at ~2000 years ago. *Acanthocythereis dunelmensis* and *Cytheropteron arcuatum* as the most important indicator species of Cluster A and Cluster B respectively are both fully marine, cold and relatively deep (lower neritic) species while another important indicator species of Cluster A, *Heterocyprideis fascis*, is euryhaline, cold and shallow species (Stepanova, 2006; Gemery et al., 2017; Stepanova et al., 2019). Coexistence of fully marine species (dominant) and euryhaline species (rare) in this period may indicate a generally saltier but highly variable environment, which is consistent with our MOSR reconstruction showing higher salinities with larger differences between maximum and minimum estimates after ~2000 yr BP. The surrounding ice sheets may have been active again to develop seasonal ice cover over Storfjorden (i.e. Neoglacial glacier advance) as indicated by peaks in IRD concentration and abundance of colder-water indicator benthic

foraminifera species *Elphidium excavatum* (Rasmussen and Thomsen, 2015). Destabilization of the oceanic and glacial conditions after ~2000 yr BP is widely indicated by other studies in Svalbard region, which show long-term cooling culminated during the Little Ice Age (LIA) to cause glacier advance (Rasmussen et al., 2012; van der Bilt et al., 2015; Farnsworth et al., 2018; Geirsdóttir et al., 2019).

6. Conclusion

Our ostracod record allows continuous observation of the Svalbard margin post-glacial emergence in higher time resolution than that of raised beach studies. We successfully reconstructed relative sea-level history in Svalbard, a near-field region, that showed the isostatic rebound of MWP-1B of ~40-80 m at~11,300–11,000 yr BP associated with the regional ice-sheet retreat possibly triggered by warm Atlantic water incursion. Low-salinity and cold conditions probably prevailed in Storfjorden with stabilization of regional ice sheets during ~11,000-2000 yr BP. Modern-like oceanographic, climatic and glacial conditions were established at ~2000 yr BP that were characterized by an active ice-sheet and perhaps even colder conditions, consistent with current understanding of Neoglacial glacier advances and cooling.

We found clear near-field evidence of MWP-1B that was previously elusive from far-field records (Lambeck et al., 2014) and not known from near-field records (Bard et al., 2010). High-resolution down-core ostracod record allows continuous reconstruction of subtidal water-depth and thus sea-level changes in a single location. This is complementary both to high-resolution, indirect sea-level records from a single location (e.g., oxygen isotope) and to direct sea-level records from many different locations (e.g.,

corals). Deglacial-Holocene sea-level studies tend to focus on far-field regions, because they record near eustatic sea-level changes with minimal isostatic effects. But near field records with sensitive indicator like ostracods can help to identify abrupt sea-level events.

Acknowledgments

We thank Dr. Colm O'Cofaigh, Dr. Thomas Cronin and an anonymous reviewer for their insightful and constructive suggestions and comments to improve this manuscript. We thank Maria Lo for her assistance in the laboratory. **Funding**: The work described in this article was partially supported by a grant from the Research Grants Council of the Hong Kong Special Administrative Region, China (project code: HKU 17311316) (to M.Y.) and by the Research Council of Norway through its Centres of Excellence funding scheme (project number: 223259) (to T. L. R.). **Author contributions**: S.Y.T. and M.Y. developed the concept; S.Y.T. performed the research with help from Y.H., H.H.M.H., H.I., W.T.R.C., B.M., H.O., T.L.R., and M.Y.; S.Y.T., Y.H., H.H.M.H., and H.I. analysed the data; S.Y.T. and M.Y. wrote the manuscript; M.Y. and Y.H. supervised the project. **Competing interests:** The authors declare that they have no competing interests.

Data and materials availability: All data needed to evaluate the conclusions in the paper are present in the Supplementary Materials and are deposited in Pangaea (DOI will be added in the proof-reading stage). Additional data related to this paper may be requested from the authors.

References

Abdul, N., Mortlock, R., Wright, J., Fairbanks, R., 2016. Younger Dryas sea level and meltwater pulse 1B recorded in Barbados reef crest coral Acropora palmata. Paleoceanography 31, 330-344.

Auriac, A., Whitehouse, P., Bentley, M., Patton, H., Lloyd, J., Hubbard, A., 2016. Glacial isostatic adjustment associated with the Barents Sea ice sheet: a modelling inter-comparison. Quaternary Science Reviews 147, 122-135.

Bard, E., Hamelin, B., Arnold, M., Montaggioni, L., Cabioch, G., Faure, G., Rougerie, F., 1996. Deglacial sea-level record from Tahiti corals and the timing of global meltwater discharge. Nature 382, 241-244.

Bard, E., Hamelin, B., Delanghe-Sabatier, D., 2010. Deglacial meltwater pulse 1B and Younger Dryas sea levels revisited with boreholes at Tahiti. Science 327, 1235-1237.

Bennington, J.B., Rutherford, S.D., 1999. Precision and reliability in paleocommunity comparisons based on cluster-confidence intervals; how to get more statistical bang for your sampling buck. Palaios 14, 506-515.

Bondevik, S., Mangerud, J., Ronnert, L., Salvigsen, O., 1995. Postglacial sea-level history of Edgeøya and Barentsøya, eastern Svalbard. Polar Research 14, 153–180.

Brouwers, E.M., 1992. Pliocene paleoecologic reconstructions based on ostracode assemblages from the Sagavanirktok and Gubik Formations, Alaskan North Slope. US Dept. of the Interior, US Geological Survey.

Cronin, T.M., 1981. Paleoclimatic implications of Late Pleistocene marine ostracodes from the St. Lawrence Lowlands. Micropaleontology 27, 384–418.

Cronin, T.M., 2015. Ostracods and sea level, in: Ian, S., Antony, L.J., Benjamin, H.P. (Eds.), Handbook of Sea-Level Research. John Wiley & Sons., pp. 249-257.

Cronin, T.M., Dwyer, G.S., Farmer, J., Bauch, H.A., Spielhagen, R.F., Jakobsson, M., Nilsson, J., Briggs Jr, W., Stepanova, A., 2012. Deep Arctic Ocean warming during the last glacial cycle. Nature Geoscience 5, 631-634.

Cronin, T.M., O'Regan, M., Pearce, C., Gemery, L., Toomey, M., Semiletov, I., Jakobsson, M., 2017. Deglacial sea level history of the East Siberian Sea and Chukchi Sea margins. Climate of the Past 13, 1097-1110.

Dimitriadou, E., Dolničar, S., Weingessel, A., 2002. An examination of indexes for determining the number of clusters in binary data sets. Psychometrika 67, 137-159.

Dowdeswell, J.A., Hogan, K., Evans, J., Noormets, R., Ó Cofaigh, C., Ottesen, D., 2010.

Past ice-sheet flow east of Svalbard inferred from streamlined subglacial landforms. Geology 38, 163-166.

Dufrêne, M., Legendre, P., 1997. Species assemblages and indicator species: the need for a flexible asymmetrical approach. Ecological monographs 67, 345-366.

Ebbesen, H., Hald, M., Eplet, T.H., 2007. Lateglacial and early Holocene climatic oscillations on the western Svalbard margin, European Arctic. Quaternary Science Reviews 26, 1999-2011.

Fairbanks, R.G., 1989. A 17,000-year glacio-eustatic sea level record: influence of glacial melting rates on the Younger Dryas event and deep-ocean circulation. Nature 342, 637-641.

Farnsworth, W.R., Ingólfsson, Ó., Retelle, M., Allaart, L., Håkansson, L.M., Schomacker, A., 2018. Svalbard glaciers re-advanced during the Pleistocene-Holocene transition. Boreas 47, 1022-1032.

Flink, A.E., Noormets, R., Fransner, O., Hogan, K.A., ÓRegan, M., Jakobsson, M., 2017. Past ice flow in Wahlenbergfjorden and its implications for late Quaternary ice sheet dynamics in northeastern Svalbard. Quaternary Science Reviews 163, 162-179.

Forman, S., Lubinski, D., Ingólfsson, Ó., Zeeberg, J., Snyder, J., Siegert, M., Matishov, G., 2004. A review of postglacial emergence on Svalbard, Franz Josef Land and Novaya Zemlya, northern Eurasia. Quaternary Science Reviews 23, 1391–1434.

Forman, S.L., 1990. Post-glacial relative sea-level history of northwestern Spitsbergen, Svalbard. Geological Society of America Bulletin 102, 1580–1590.

Geirsdóttir, Á., Miller, G.H., Andrews, J.T., Harning, D.J., Anderson, L.S., Florian, C., Larsen, D.J., Thordarson, T., 2019. The onset of Neoglaciation in Iceland and the 4.2 ka event. Climate of the Past 15, 25-40.

Gemery, L., Cronin, T.M., Briggs, W.M., Brouwers, E.M., Schornikov, E.I., Stepanova, A., Wood, A.M., Yasuhara, M., 2017. An Arctic and Subarctic ostracode database: biogeographic and paleoceanographic applications. Hydrobiologia 786, 59-95.

Gjermundsen, E.F., Briner, J.P., Akçar, N., Salvigsen, O., Kubik, P., Gantert, N., Hormes, A., 2013. Late Weichselian local ice dome configuration and chronology in Northwestern Svalbard: early thinning, late retreat. Quaternary Science Reviews 72, 112-127.

Hald, M., Ebbesen, H., Forwick, M., Godtliebsen, F., Khomenko, L., Korsun, S., Olsen, L.R., Vorren, T.O., 2004. Holocene paleoceanography and glacial history of the West Spitsbergen area, Euro-Arctic margin. Quaternary Science Reviews 23, 2075–2088.

Harrison, S., Smith, D.E., Glasser, N.F., 2019. Late Quaternary meltwater pulses and sea level change. Journal of Quaternary Science 34, 1-15.

Hartigan, J.A., Wong, M.A., 1979. Algorithm AS 136: A k-means clustering algorithm. Journal of the Royal Statistical Society. Series C (Applied Statistics) 28, 100-108.

Hogan, K., Dowdeswell, J., Noormets, R., Evans, J., Cofaigh, C.Ó., Jakobsson, M., 2010. Submarine landforms and ice-sheet flow in the Kvitøya Trough, northwestern Barents Sea. Quaternary Science Reviews 29, 3545-3562.

Hong, Y., Yasuhara, M., Iwatani, H., Mamo, B., 2019. Baseline for ostracod-based northwestern Pacific and Indo-Pacific shallow-marine paleoenvironmental reconstructions: ecological modeling of species distributions. Biogeosciences 16, 585–604.

Horne, D.J., 2007. A mutual temperature range method for Quaternary palaeoclimatic analysis using European nonmarine Ostracoda. Quaternary Science Reviews 26, 1398-1415.

Ingolfsson, O., Landvik, J.Y., 2013. The Svalbard–Barents Sea ice-sheet–Historical, current and future perspectives. Quaternary Science Reviews 64, 33-60.

Khan, N.S., Ashe, E., Shaw, T.A., Vacchi, M., Walker, J., Peltier, W., Kopp, R.E., Horton, B.P., 2015. Holocene relative sea-level changes from near-, intermediate-, and far-field locations. Current Climate Change Reports 1, 247-262.

Knies, J., Pathirana, I., Cabedo-Sanz, P., Banica, A., Fabian, K., Rasmussen, T.L., Forwick, M., Belt, S.T., 2016. Sea-ice dynamics in an Arctic coastal polynya during the past 6500 years. arktos 3, https://doi.org/10.1007/s41063-41016-40027-y.

Łącka, M., Zajączkowski, M., Forwick, M., Szczuciński, W., 2015. Late Weichselian and Holocene palaeoceanography of Storfjordrenna, southern Svalbard. Climate of the Past 11, 587-603.

Lambeck, K., Rouby, H., Purcell, A., Sun, Y., Sambridge, M., 2014. Sea level and global ice volumes from the Last Glacial Maximum to the Holocene. Proceedings of the National Academy of Sciences 111, 15296–15303.

Long, A.J., Strzelecki, M.C., Lloyd, J.M., Bryant, C.L., 2012. Dating High Arctic Holocene relative sea level changes using juvenile articulated marine shells in raised beaches. Quaternary Science Reviews 48, 61–66.

Lord, A., 1980. Weichselian (Late Quaternary) ostracods from the Sandnes Clay, Norway. Geological Magazine 117, 227-242.

Mayewski, P.A., Rohling, E.E., Stager, J.C., Karlén, W., Maasch, K.A., Meeker, L.D.,

Meyerson, E.A., Gasse, F., van Kreveld, S., Holmgren, K., 2004. Holocene climate variability. Quaternary research 62, 243-255.

Milne, G.A., Mitrovica, J.X., 2008. Searching for eustasy in deglacial sea-level histories. Quaternary Science Reviews 27, 2292-2302.

Nielsen, T., Rasmussen, T.L., 2018. Reconstruction of ice sheet retreat after the Last Glacial maximum in Storfjorden, southern Svalbard. Marine Geology 402, 228-243.

Patton, H., Hubbard, A., Andreassen, K., Auriac, A., Whitehouse, P.L., Stroeven, A.P., Shackleton, C., Winsborrow, M., Heyman, J., Hall, A.M., 2017. Deglaciation of the Eurasian ice sheet complex. Quaternary Science Reviews 169, 148-172.

Penney, D.N., 1989. Recent shallow marine ostracoda of the Ikerssuak (Bredefjord) district, Southwest Greenland. Journal of Micropalaeontology 8, 55-75.

Penney, D.N., 1993. Northern North Sea benthic Ostracoda: modern distribution and palaeoenvironmental significance. The Holocene 3, 241–244.

Rasmussen, T.L., Forwick, M., Mackensen, A., 2012. Reconstruction of inflow of Atlantic Water to Isfjorden, Svalbard during the Holocene: Correlation to climate and seasonality. Marine Micropaleontology 94, 80-90.

Rasmussen, T.L., Thomsen, E., 2014. Brine formation in relation to climate changes and ice retreat during the last 15,000 years in Storfjorden, Svalbard, 76–78 N. Paleoceanography 29, 911–929.

Rasmussen, T.L., Thomsen, E., 2015. Palaeoceanographic development in Storfjorden, Svalbard, during the deglaciation and Holocene: evidence from benthic foraminiferal records. Boreas 44, 24–44.

Schoning, K., Wastegård, S., 1999. Ostracod assemblages in late Quaternary varved glaciomarine clay of the Baltic Sea Yoldia stage in eastern middle Sweden. Marine Micropaleontology 37, 313-325.

Skogseth, R., Haugan, P., Haarpaintner, J., 2004. Ice and brine production in Storfjorden from four winters of satellite and in situ observations and modeling. Journal of Geophysical Research: Oceans 109, https://doi.org/10.1029/2004JC002384.

Skogseth, R., Haugan, P., Jakobsson, M., 2005. Watermass transformations in Storfjorden. Continental Shelf Research 25, 667-695.

Stanford, J.D., Hemingway, R., Rohling, E.J., Challenor, P.G., Medina-Elizalde, M., Lester, A.J., 2011. Sea-level probability for the last deglaciation: A statistical analysis of far-field records. Global and Planetary Change 79, 193-203.

Stepanova, A., Obrochta, S., Quintana Krupinski, N.B., Hyttinen, O., Kotilainen, A.,

Andrén, T., 2019. Late Weichselian to Holocene history of the Baltic Sea as reflected in ostracod assemblages. Boreas 48, 761-778.

Stepanova, A., Taldenkova, E., Bauch, H.A., 2003. Recent Ostracoda from the Laptev Sea (Arctic Siberia): species assemblages and some environmental relationships. Marine Micropaleontology 48, 23–48.

Stepanova, A., Taldenkova, E., Bauch, H.A., 2012. Ostracod palaeoecology and environmental change in the Laptev and Kara seas (Siberian Arctic) during the last 18000 years. Boreas 41, 557-577.

Stepanova, A., Taldenkova, E., Simstich, J., Bauch, H.A., 2007. Comparison study of the modern ostracod associations in the Kara and Laptev seas: Ecological aspects. Marine Micropaleontology 63, 111–142.

Stepanova, A.Y., 2006. Late Pleistocene-Holocene and Recent Ostracoda of the Laptev Sea and their importance for paleoenvironmental reconstructions. Paleontological Journal 40, S91–S204.

van der Bilt, W.G., Bakke, J., Vasskog, K., D'Andrea, W.J., Bradley, R.S., Ólafsdóttir, S., 2015. Reconstruction of glacier variability from lake sediments reveals dynamic Holocene climate in Svalbard. Quaternary Science Reviews 126, 201-218.

Whatley, R., Eynon, M., Moguilevsky, A., 1996. Recent ostracoda of the Scoresby Sund fjiord system, east Greenland. Revista Española de Micropaleontología 28, 5-24.

Whatley, R., Eynon, M., Moguilevsky, A., 1998. The depth distribution of Ostracoda from the Greenland Sea. Journal of Micropalaeontology 17, 15-32.

Whatley, R., Masson, D., 1979. The ostracod genus Cytheropteron from the Quaternary and Recent of Great Britain. Revista Espanola de Micropaleontologia 11, 223–277.

Yasuhara, M., Iwatani, H., Hunt, G., Okahashi, H., Kase, T., Hayashi, H., Irizuki, T., Aguilar, Y.M., Fernando, A.G.S., Renema, W., 2017. Cenozoic dynamics of shallow-marine biodiversity in the Western Pacific. Journal of Biogeography 44, 567–578.

Yasuhara, M., Seto, K., 2006. Holocene relative sea-level change in Hiroshima Bay, Japan: a semi-quantitative reconstruction based on ostracodes. Paleontological Research 10, 99-116.

Yasuhara, M., Stepanova, A., Okahashi, H., Cronin, T.M., Brouwers, E.M., 2014. Taxonomic revision of deep-sea Ostracoda from the Arctic Ocean. Micropaleontology 60, 399-444.

Yasuhara, M., Yoshikawa, S., Nanayama, F., 2005. Reconstruction of the Holocene seismic history of a seabed fault using relative sea-level curves reconstructed by

ostracode assemblages: Case study on the Median Tectonic Line in Iyo-nada Bay, western Japan. Palaeogeography, Palaeoclimatology, Palaeoecology 222, 285-312.
Yokoyama, Y., Esat, T.M., Thompson, W.G., Thomas, A.L., Webster, J.M., Miyairi, Y., Sawada, C., Aze, T., Matsuzaki, H., Okuno, J.i., 2018. Rapid glaciation and a two-step sea level plunge into the Last Glacial Maximum. Nature 559, 603-607.

Tables and figure captions

Table 1. Indicator Value scores of ostracod species for each cluster and corresponding p-value.

Species	Cluster A	Cluster B	Cluster C	Cluster D	p-value
Acanthocythereis dunelmensis	0.958717	0.002506	0.002176	0	0.001
Argilloecia sp A	0.075352	0.006367	0.146314	0	0.233
Argilloecia sp B	0	0.013717	0.043805	0	0.604
Bythocythere constricta	0	0.148346	0.004856	0	0.047
Cluthia cluthae	0.053578	0.307193	0.094853	0	0.023
Cytheropteron arcuatum	0	0.450434	0.184302	0.007909	0.002
Cytheropteron biconvexa	0.066882	0.103582	0.259639	0.012386	0.107
Cytheropteron dimlingtonensis	0.256061	0.087882	0.00482	0.282091	0.044
Cytheropteron discoveria	0.303358	0.009527	0.002878	0	0.001
Cytheropteron inflatum	0.002161	0.175862	0.059062	0.085325	0.308
Cytheropteron irizukii	0	0.00201	0.002067	0.158587	0.026
Cytheropteron laptevensis	0	0.082765	0.015655	0.01296	0.352

Cytheropteron montrosiense	0	0.116478	0	0.189822	0.019
Cytheropteron nodosum	0.009073	0.001858	0.009315	0.121573	0.095
Cytheropteron nodosoalatum	0.124894	0.107746	0.044409	0	0.519
Cytheropteron paralatissimum	0.017583	0.257464	0.005404	0.22343	0.032
Cytheropteron pseudomontrosiense	0	0.034015	5.77E-06	0.905081	0.001
Cytheropteron tumefactum	0	0.155239	0.006995	0.010807	0.044
Elofsonella concinna	0	0.052374	0.472403	0	0.001
Heterocyprideis fascis	0.385669	0.133498	0.001291	0	0.003
Heterocyprideis sorbyana	0	0.037709	0.205298	0.008624	0.072
Krithe glacialis	0	0.125621	0.042817	0.095453	0.318
Loxoconcha spp	0	0.062959	0	0.043213	0.233
Normanicythere leioderma	0	0.01196	0.742277	0.00497	0.001
Pseudocythere caudata	0	0.0321	0.010533	0	0.8
Rabilimis mirabilis	0	0	0.08	0	0.233
Sarsicytheridea bradii	0.217476	0.080423	0.518348	0	0.001
Sarsicytheridea punctillata	0	0.010957	0.869599	0	0.001
Semicytherura complanata	0.128733	0.257017	0.12248	0	0.088
Semicytherura concentrica	0	0.149904	0.001683	0	0.036

Table 2. Autoecology summary of indicator species and *Krithe glacialis*.

Species	Cluster	Autoecology	References
Acanthocythereis dunelmensis, *Cytheropteron discoveria*	A	Relatively deep (lower neritic) and cold water, full marine	(Stepanova et al., 2003; Stepanova, 2006; Gemery et al., 2017; Stepanova et al., 2019)
Heterocyprideis fascis	A	Shallow (neritic) and cold water, euryhaline	(Brouwers, 1992; Gemery et al., 2017)
Bythocythere constricta, *Cluthia cluthae*, *Cytheropteron arcuatum*, *Cytheropteron tumefactum*, *Semicytherura concentrica*	B	Relatively deep (lower neritic) and cold water, full marine	(Penney, 1989; Brouwers, 1992; Stepanova et al., 2003; Stepanova et al., 2007; Stepanova et al., 2012; Stepanova et al., 2019)
Cytheropteron paralatissimum	B	Cold water, full marine	(Lord, 1980; Brouwers, 1992)
Elofsonella concinna, *Sarsicytheridea punctillata*, *Sarsicytheridea bradii*	C	Shallow (neritic) and cold water, euryhaline	(Cronin, 1981; Penney, 1993; Stepanova et al., 2003; Stepanova, 2006; Stepanova et al., 2012; Stepanova et al., 2019)

Normanicythere leioderma	C	Shallow (neritic) and cold water, full marine	(Gemery et al., 2017; Stepanova et al., 2019)
Krithe glacialis		Deep (uppermost bathyal) and warm water, full marine	(Whatley et al., 1998; Stepanova, 2006)
Cytheropteron montrosiense	D	Shallow (neritic) and cold water	(Brouwers, 1992; Stepanova, 2006)
Cytheropteron dimlingtonensis	D	Deep (lower neritic to uppermost bathyal) and cold water, full marine	(Whatley and Masson, 1979; Stepanova, 2006)
Cytheropteron irizukii	D	Deep (bathyal) and cold water	(Yasuhara et al., 2014)
Cytheropteron pseudomontrosiense	D	Deep (upper bathyal) and cold water, full marine	(Stepanova et al., 2003; Stepanova, 2006; Stepanova et al., 2019)

Table 3. Summary of paleobathymetry (shown by orange box) of Clusters A–D.

		Paleobathymetry		
Cluster	Indicator species	Upper neritic-middle neritic	Lower neritic	Bathyal
A	*Acanthocythereis dunelmensis* *Cytheropteron discoveria* *Heterocyprideis fascis*			
B	*Bythocythere constricta* *Cluthia cluthae* *Cytheropteron arcuatum* *Cytheropteron paralatissimum* *Cytheropteron tumefactum* *Semicytherura concentrica*			

C	*Elofsonella concinna* *Normanicythere leioderma* *Sarsicytheridea punctillata* *Sarsicytheridea bradii*			
D	*Cytheropteron dimlingtonensis* *Cytheropteron irizukii* *Cytheropteron montrosiense* *Cytheropteron pseudomontrosiense*			

Fig. 1. Map of Storfjorden, Svalbard, the Arctic Ocean.

This map shows position of Sites JM10-10GC and JM10-12GC (black circles indicated as 10 and 12, respectively) and main ocean currents (warm Atlantic water by red arrows and cold polar water by blue arrows). Tow bathymetric lines indicate water depth of 100 m and 200 m respectively across the studied area.

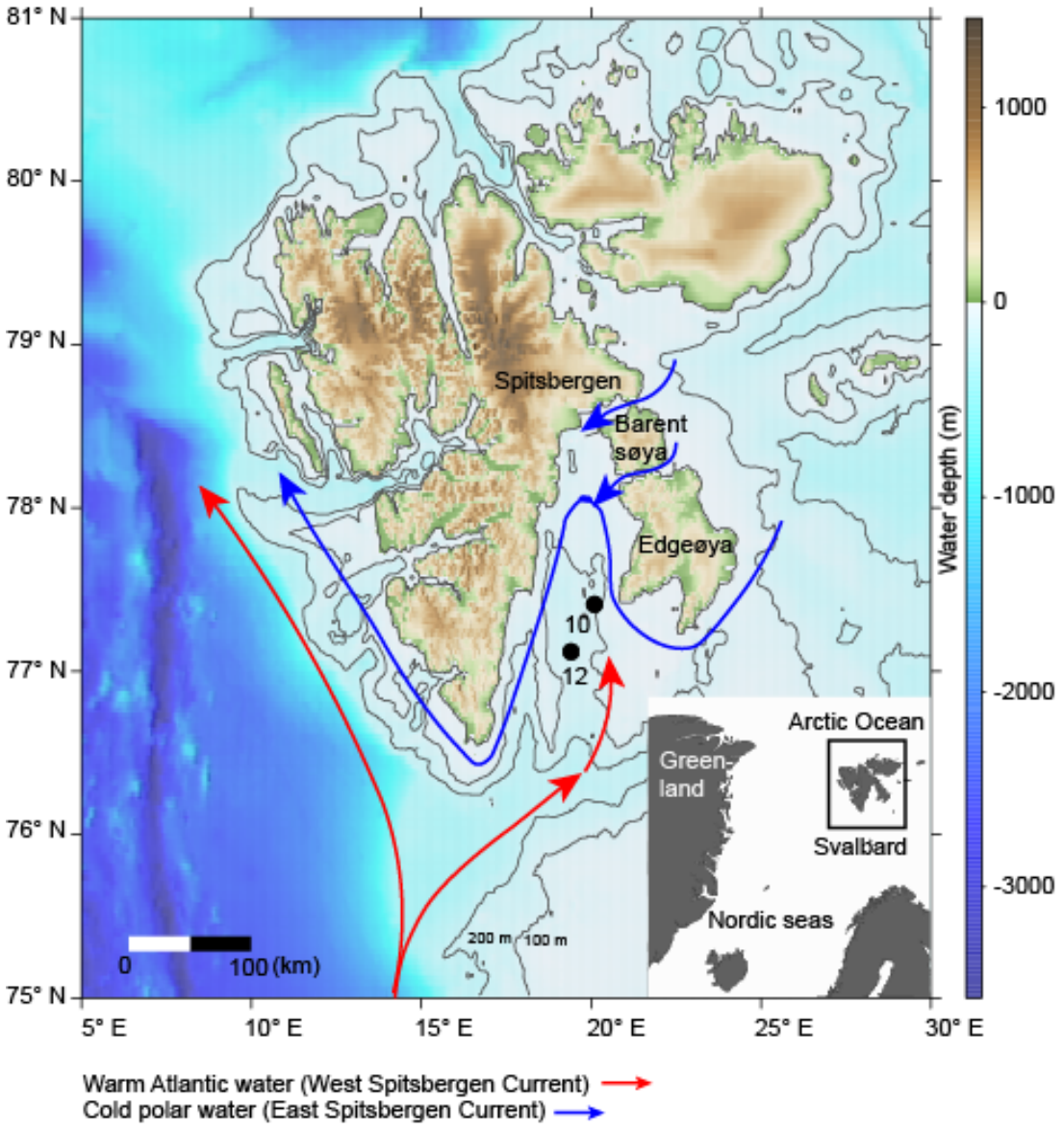

Fig. 2. Two examples of the application of MODR method to reconstruct paleo water depth in Cores JM10-10GC and JM10-12GC.

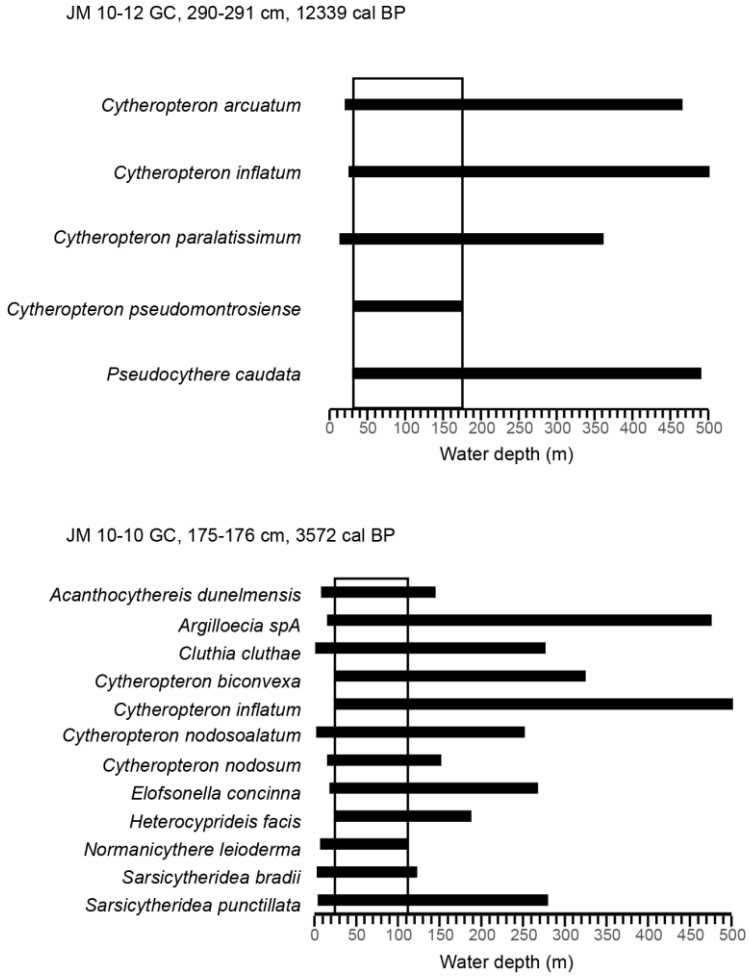

Fig. 3. Relative abundance plots of Clusters A, B, C and D indicator species and *Krithe glacialis*. Samples of low abundance (less than 10 specimens) are excluded. Color bar indicates horizon of each sample that belongs to Clusters A (orange), B (blue), C (red), or D (green). MWP-1B is indicated by (A) the grey bar spanning 11,300-10,500 yr BP in Core JM10-10GC (B) the grey bar spanning 11,300-11,000 yr BP in Core JM10-12GC. Cluster D-Cluster B-Cluster C-Cluster A succession reflects three-stage paleoenvironmental transitions (i.e. before ~11,000 yr BP, ~11,000-2000 yr BP, after ~2000 yr BP) from the last deglaciation to late Holocene.

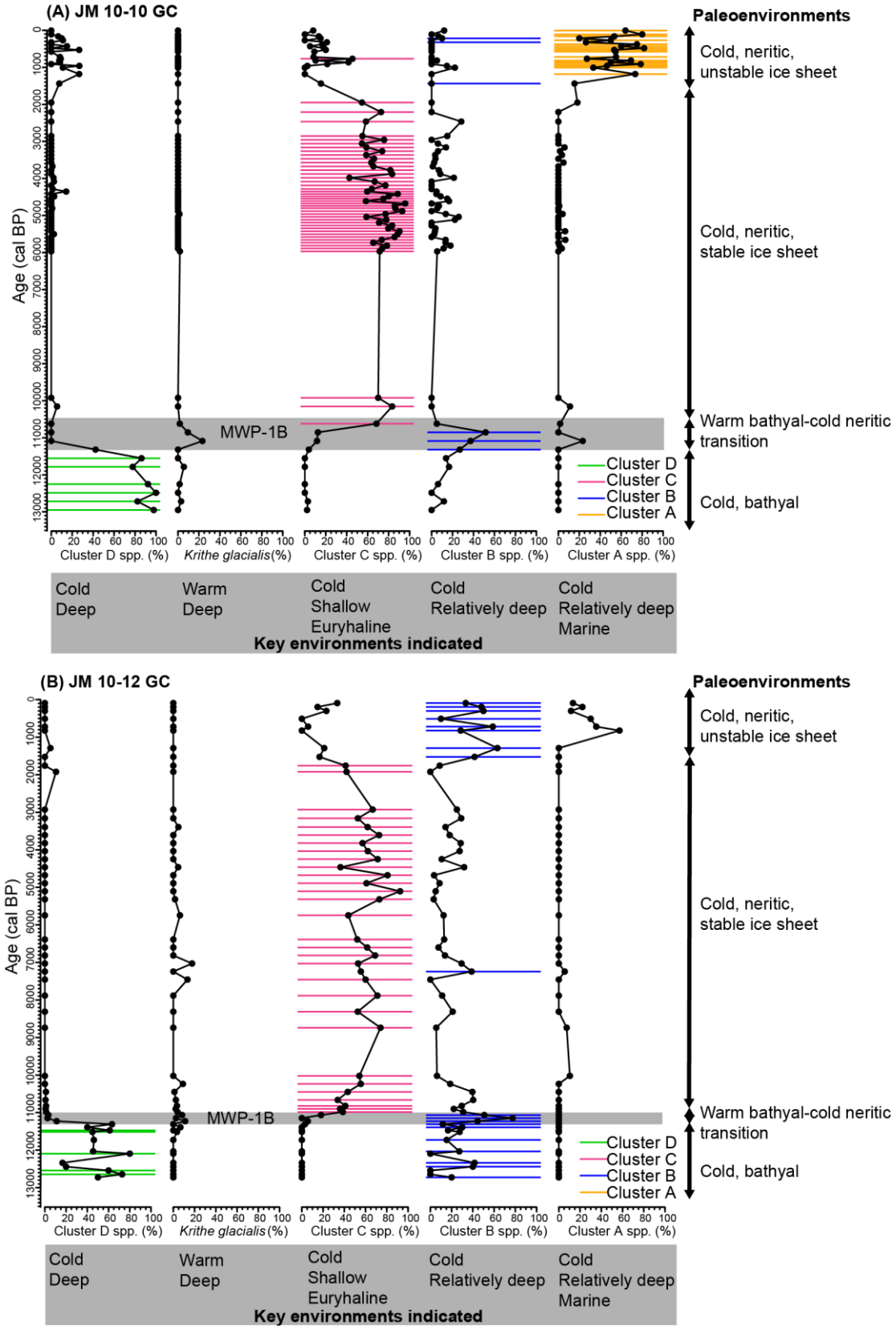
(A) JM 10-10 GC
Paleoenvironments
Cold, neritic, unstable ice sheet
Cold, neritic, stable ice sheet
Warm bathyal-cold neritic transition
Cold, bathyal
Age (cal BP)
MWP-1B
Cluster D
Cluster C
Cluster B
Cluster A
Cluster D spp. (%)
Krithe glacialis(%)
Cluster C spp. (%)
Cluster B spp. (%)
Cluster A spp. (%)
Cold Deep
Warm Deep
Cold Shallow Euryhaline
Cold Relatively deep
Cold Relatively deep Marine
Key environments indicated
(B) JM 10-12 GC
Paleoenvironments
Cold, neritic, unstable ice sheet
Cold, neritic, stable ice sheet
Warm bathyal-cold neritic transition
Cold, bathyal
Age (cal BP)
MWP-1B
Cluster D
Cluster C
Cluster B
Cluster A
Cluster D spp. (%)
Krithe glacialis(%)
Cluster C spp. (%)
Cluster B spp. (%)
Cluster A spp. (%)
Cold Deep
Warm Deep
Cold Shallow Euryhaline
Cold Relatively deep
Cold Relatively deep Marine
Key environments indicated

Fig. 4. Indicator value scores and p-values of Clusters A to D indicator species. Statistically significant indicator species of each cluster are highlighted by corresponding color used in Figure 3. The scores are available in Table 1.

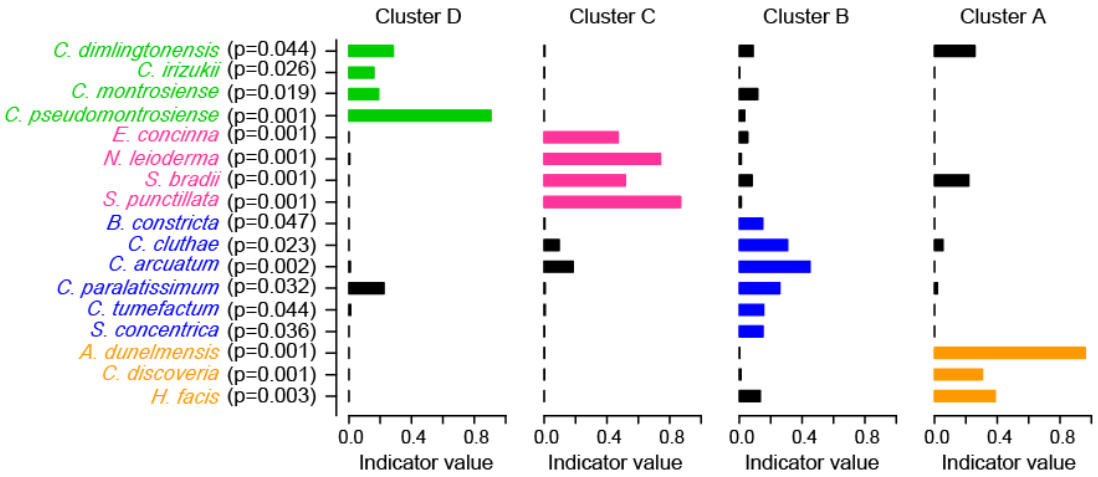

Fig. 5. Plots of relative abundance of important ostracod species in Core JM10-10GC. Samples of low abundance (less than 10 specimens) are excluded. Indicator species of Clusters A, B, C and D are highlighted by corresponding color used in Figure 3.

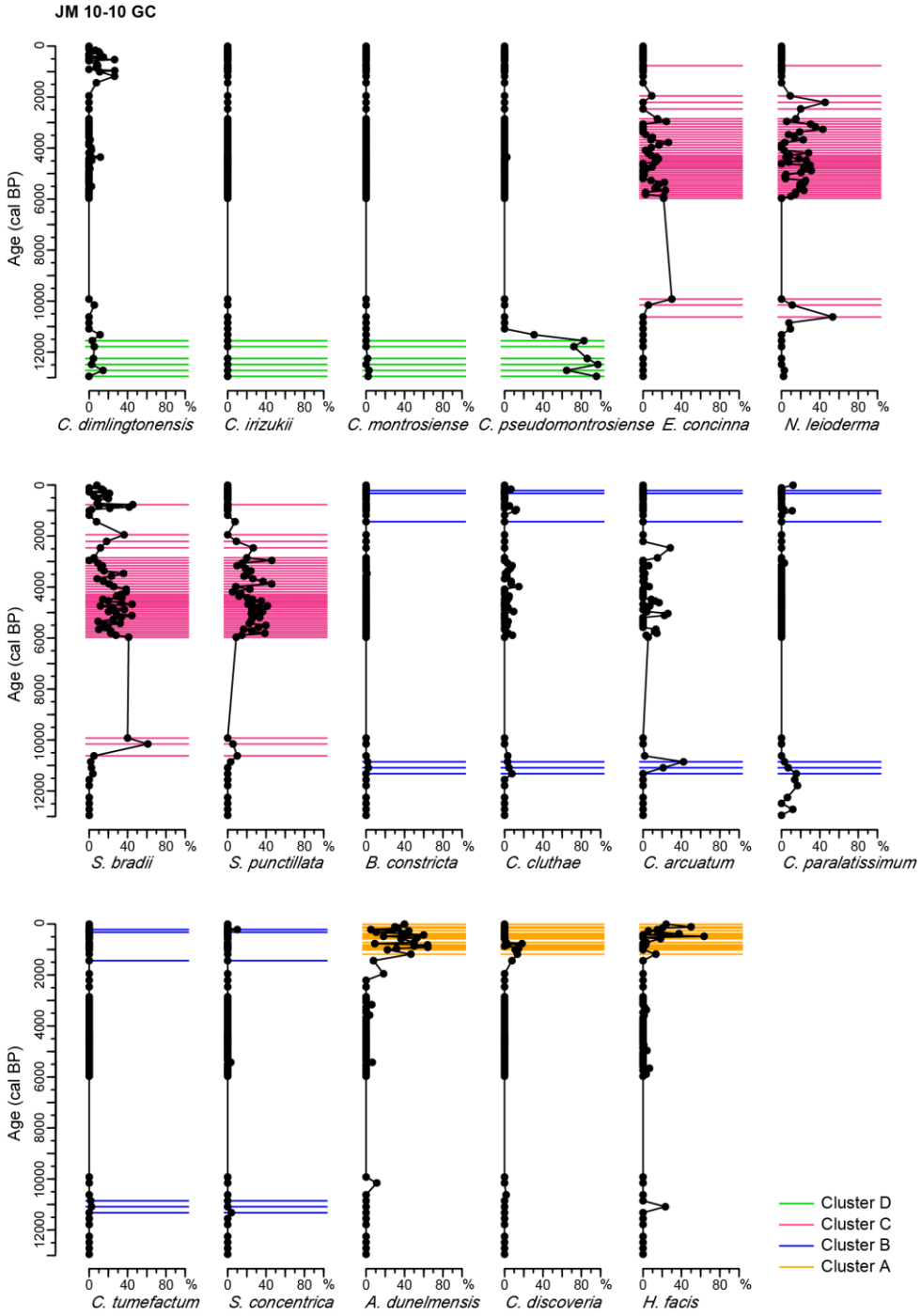

Fig. 6. Plots of relative abundance of important ostracod species in Core JM10-12GC. Samples of low abundance (less than 10 specimens) are excluded. Indicator species of Clusters A, B, C and D are highlighted by corresponding color used in Figure 3.

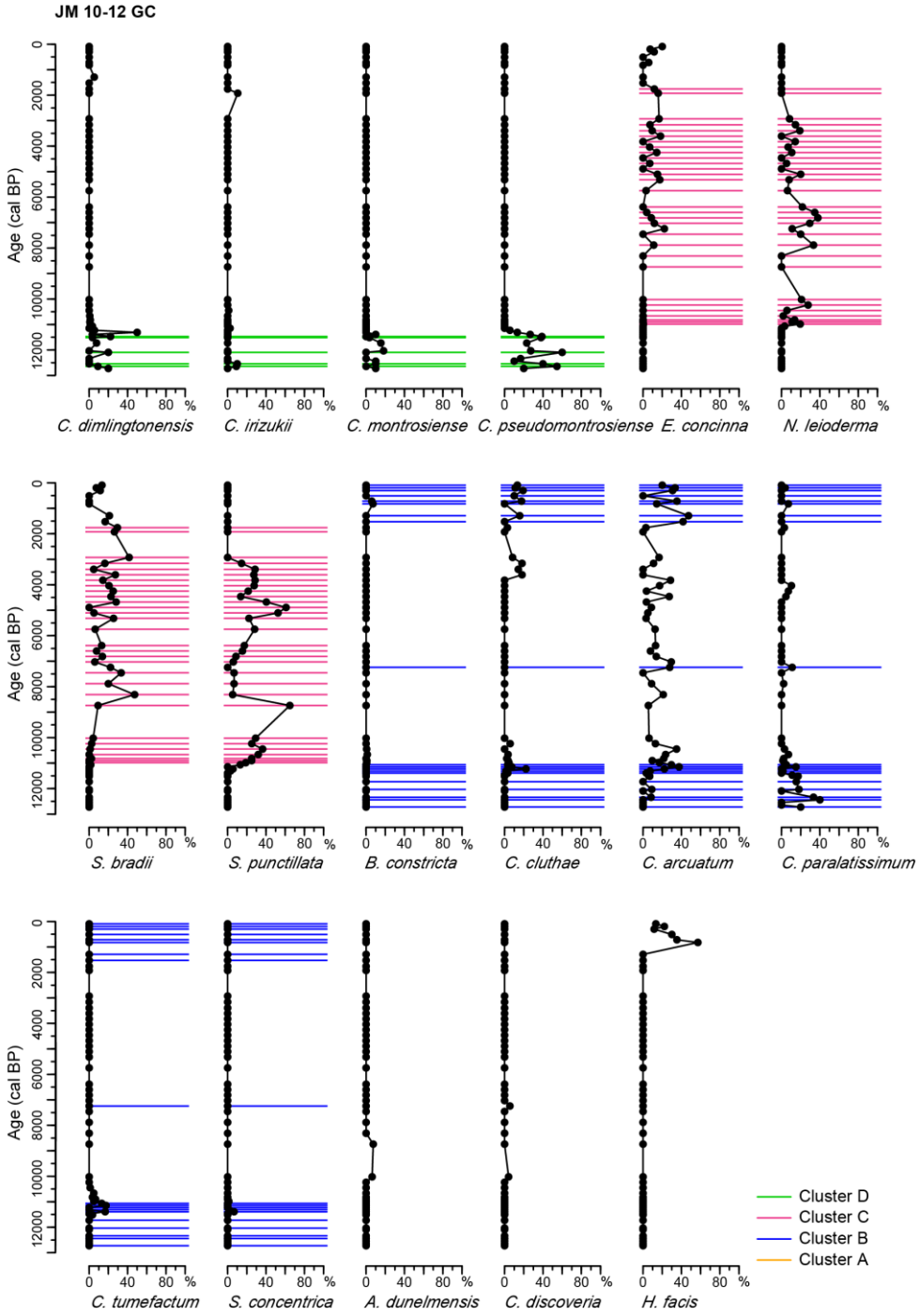

Fig. 7. MODR reconstructions of paleo water depth for Cores (A) JM10-10GC and (B) JM10-12GC. Maximal and minimal estimations of water depth are plotted in orange and blue respectively, of which maximal estimation is interpreted as actual paleo-depth. The MWP-1B interval is highlighted by gray bars. The black arrows indicate the rapid RSL fall from pre- to post-MWP-1B.

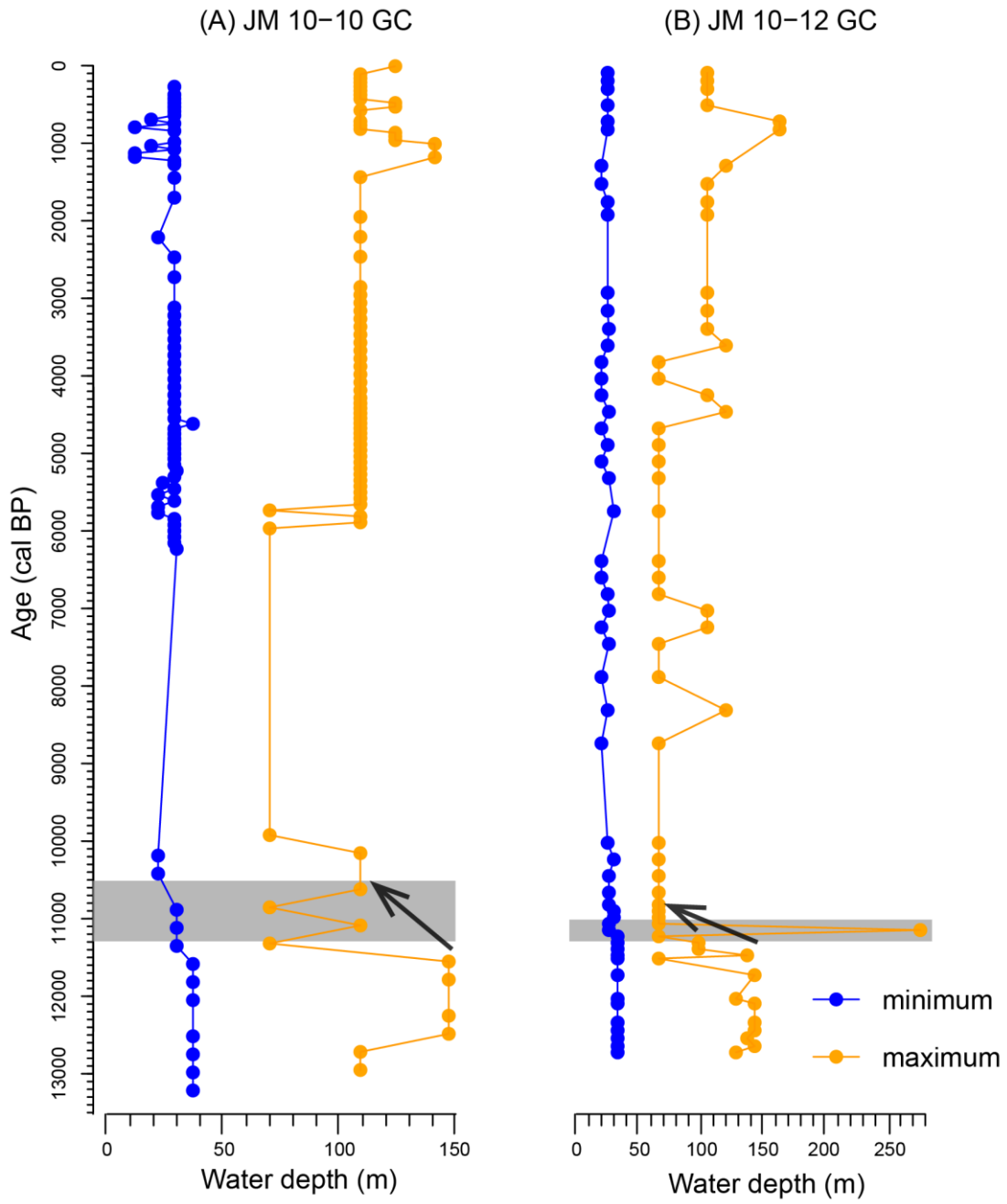

Fig. 8. MOSR reconstructions of paleo salinities for Cores (A) JM10-10GC and (B) JM10-12GC. Maximal and minimal estimations of salinity are plotted in orange and blue respectively. Each grey bar indicates one missing data horizon for which MOSR method fails to give the corresponding salinity range (see Method section).

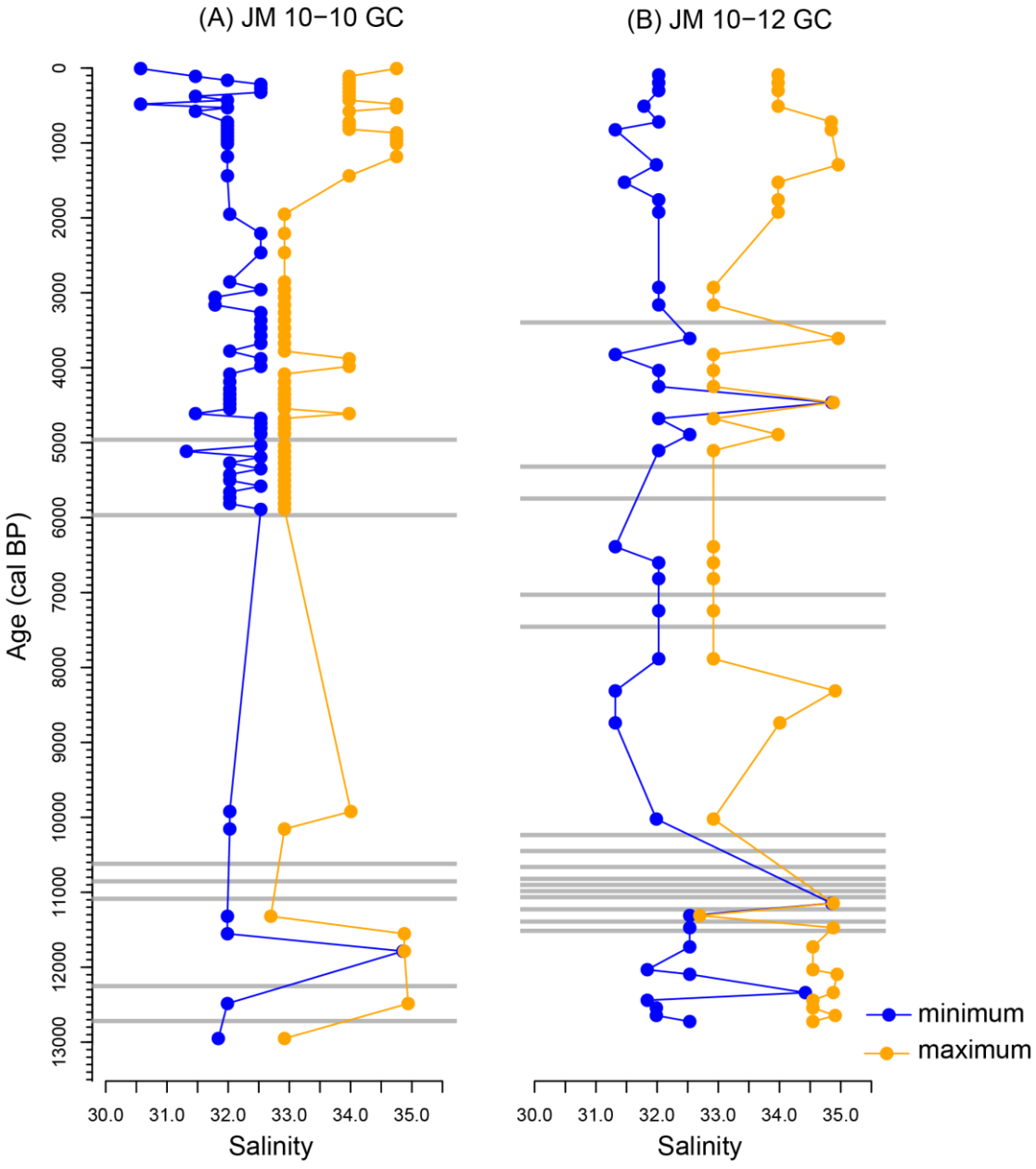

Fig. 9. *Krithe glacialis* relative abundance and total number of planktonic foraminiferan specimens per sample for Cores (A) JM10-10GC and (B) JM10-12GC. Samples of low ostracod abundance (less than 10 specimens) are excluded from the relative abundance plots of *Krithe glacialis*.